

Collisional Effects on Nonlinear Ion Drag Force for Small Grains

I H Hutchinson¹ and C B Haakonsen¹

*Plasma Science and Fusion Center and
Department of Nuclear Science and Engineering,
Massachusetts Institute of Technology,
Cambridge, MA, USA.*

The ion drag force arising from plasma flow past an embedded spherical grain is calculated self-consistently and non-linearly using particle in cell codes, accounting for ion-neutral collisions. Using ion velocity distribution appropriate for ion drift driven by a force field gives wake potential and force greatly different from a shifted Maxwellian distribution, regardless of collisionality. The low-collisionality forces are shown to be consistent with estimates based upon cross-sections for scattering in a Yukawa (shielded) grain field, but only if non-linear shielding length is used. Finite collisionality initially enhances the drag force, but only by up to a factor of 2. Larger collisionality eventually reduces the drag force. In the collisional regime, the drift distribution gives larger drag than the shift distribution even at velocities where their collisionless drags are equal. Comprehensive practical analytic formulas for force that fit the calculations are provided.

I. INTRODUCTION

The drag force arising from the interaction of flowing ions with a negatively charged grain embedded in a plasma has been the subject of intensive study during the recent past. It is a problem of substantial intrinsic interest as well the basis for understanding much of the behavior of grain equilibrium and dynamics in dusty plasmas. Yet reliable values for the drag in collisional plasmas are still not known.

Neglecting ion-neutral and ion-electron collisions, the classic Coulomb orbit impact parameter integral treatment¹⁻³, used for the plasma particles themselves, can be applied to a grain when the plasma electron Debye length (λ_{De}) is sufficiently large compared with the grain radius (r_p). Strictly speaking, it is when λ_{De} is much greater than the 90-degree scattering impact parameter for a typical ion velocity (v_i),

$$b_{90} \equiv \frac{Ze|Q|}{4\pi\epsilon_0 m_i v_i^2}, \quad (1)$$

where m_i , Z are the ion mass and charge-number, and Q is the charge on the grain. However, for dust grains (unlike elementary particles) r_p and hence Q are usually large enough that b_{90}/λ_{De} is not small, and so the standard treatment is inapplicable, because the argument of the Coulomb logarithm is not large. For example if $Z = 1$, $\lambda_{De} \sim 600\mu\text{m}$, $T_e/T_i \sim 100$ and grain potential is $\phi_p \sim -2T_e/e$, representing a typical dusty plasma experiment, then at the ion thermal velocity, $b_{90}/\lambda_{De} \sim 2(r_p/\lambda_{De})(T_e/T_i) \sim r_p/3\mu\text{m}$. In such a plasma, even for grains at the lower limit of being able to be detected by unperturbative laser illumination (optimistically perhaps $r_p \sim 0.3\mu\text{m}$), b_{90}/λ_{De} is too large for the cut-off Coulomb logarithm to give accurate results⁴. Practically all dusty plasma experiments with approximately room-temperature ions are in the non-linear regime $b_{90}/\lambda_{De} \gtrsim 1$.

Ions moving with superthermal directed velocity exhibit smaller b_{90} . For example, at the sound speed a value $b_{90}/\lambda_{De} \sim 2(r_p/\lambda_{De})$ results (smaller by T_i/T_e), which would not usually imply strong nonlinearity. However, as we shall see in a moment, the correct distribution function for ions whose drift is driven by electric field against drag arising from neutral collisions, is *not* a shifted Maxwellian at the flow speed. Instead the distribution retains a substantial fraction of its population at low ion speed, and hence still in the non-linear regime $b_{90}/\lambda_{De} \gtrsim 1$.

If the shielded potential of the grain is approximated by a Debye-Hückel (Yukawa) form $\phi = \phi_p \exp[-(r - r_p)/\lambda] r_p/r$, then, even into the nonlinear regime ($b_{90}/\lambda_{De} > 1$), one can

calculate the momentum transfer cross-section as a function of ion velocity by integrating (generally numerically) ion orbits^{5–9}. However, even if this potential remains valid, despite the inadequacy of the linearized Boltzmann approximation on which the Yukawa form is based, it is unclear exactly what value to use for the shielding length (λ) even though some important studies^{10,11} address the question. This is especially difficult for $T_e/T_i \gg 1$, since the ions then dominate the shielding length. Moreover, direct absorption of ions that strike the grain must be accounted for.

The self-consistent ion drag force on a single grain in a *collisionless* plasma has previously been determined from particle-in-cell calculations^{12,13} (using the code SCEPTIC), as a function of the flow velocity v_f of a shifted Maxwellian ion distribution, over a range of values of λ_{De}/r_p , T_e/T_i , for electrically floating grains. The values differ significantly (up to factor of 2) from the best binary collision calculations^{9,14,15}. The differences arise because the shielded potential form assumed in those theories is not what actually occurs. There are important spherical-asymmetries in the ion density and potential that are not accounted for by the heuristic potential assumptions. A practical numerical expression¹³, which approximates the PIC calculations, covers most of the relevant parameter space for collisionless plasmas with shifted Maxwellian ions.

A major shortcoming of collisionless drag force calculations is that many experiments are carried out in regimes where ion-neutral collisions are important. The neutral density in many dusty plasma experiments is such that charge-exchange collisions between ions and neutrals can occur with mean-free-path less than λ_{De} . For example, in argon gas pressures between 10 and 100 Pa, the typical collision mean free path is in the approximate range 1mm to 0.1mm. Collisionless treatments are therefore suspect, and the question arises as to what effects collisions have.

Actually, even for very low collisionalities the collisions can be important. The most important effect is that the velocity distribution of ions is not a shifted Maxwellian in a situation where the drift is driven by a force field (for example background electric field) in a *stationary neutral* background^{16–20}. The change of the distribution function form is independent of the level of collisionality. It occurs formally even in the low-collisionality limit. For ion drift that exceeds the neutral thermal speed (very often the case) the resulting distribution retains, for example, a substantial fraction of the ions with velocities near the (neutral) thermal velocity $v_i \sim v_{th}$, which is not the case with a shifted Maxwellian. This

difference of ion distribution alone has important effects on the ion drag force.

Taking into account a finite level of collisionality brings into play effects that have so far defied incorporation into the binary collision treatment. As an alternative, kinetic-theory calculations that utilize the linearized plasma response²¹ have been pursued^{18,22}, which can incorporate both the non-Maxwellian background ion distribution, and the direct effects of collisions. Unfortunately these calculations confront the fact that most experimental dusty plasma parameters are not such as to justify the linear approximation. The wave-number integrations that the linearized response utilizes must be heuristically cut off to prevent unphysical divergences, and the argument of the resulting logarithmic factor is $\sim \lambda_{De}/b_{90}$: not large. The quantitative results are therefore unreliable.

Again some SCEPTIC calculations¹⁹ have given fully self-consistent values of the force incorporating both the correct background distribution and the direct effects of collisions. These results have contradicted some of the speculations about self-acceleration of dust grains, showing that while it is indeed possible for the ion drag force to reverse direction, it does so only deep into the strongly collisional (short-mean-free-path) regime where other forces on the grain are dominant. However, these simulations have so far been limited to sound-speed level drift velocities, and no comprehensive practical fit to the collisional drag force has yet been developed.

In the mean time, the wake potential structure²³⁻²⁷ has been under investigation in order better to understand the mutual interaction of multiple grains^{28,29}. Most such calculations have so far used shifted Maxwellian ion distributions. However, the non-Maxwellian character expected with even vanishingly small level of collisionality has a major effect on the wake structure because it completely changes (generally greatly enhances) the Landau damping which is usually responsible for the decay of the potential oscillations.

The purpose of the present article is to provide a wide ranging numerical exploration of the consequences of charge-exchange neutral collisions for the ion drag on a small grain in a uniform, drifting-ion plasma, accounting fully for the non-linearity of the problem. The effects of the ion distribution function shape changes are documented separately from the collisionality itself, and relatively small flow velocities as well as sonic and supersonic investigated. Because of the rather large number of relevant parameters even ignoring any magnetic field (as we do here) the coverage of the parameter space is limited. In particular for our comprehensive investigations we treat only the case $T_e/T_i = 100$, which is the upper

end of the applicable temperature ratio range, and we choose to fix the grain potential to $\phi_p = -2T_e/e$, a typical floating value.

Section II explains the computational techniques and outlines the analytic treatments that are to be compared with the simulations. Section III compares the plasma shielding/wake character observed in computational simulations for the shifted Maxwellian and driven-drift non-Maxwellian background ion distributions. It also documents the ion drag force for negligible level of collisionality and demonstrates the sufficiency of the analytic collisionless ‘fits’. In engineering parlance these fits are empirical ‘correlations’ though motivated by the underlying physics. Section IV contains the numerical simulation results for a wide range of collisionality, developing a practical fit to express the influence of collisions as a correction factor for the ion drag force relative to the collisionless value. Section V offers a heuristic explanation of the calculated trends with collisionality.

II. TECHNIQUES, THEORY, AND COLLISIONLESS FITS

A. Particles in Cell

The particle in cell computational approach to representing the interaction of the flowing plasma with a spherical grain has been described in detail elsewhere^{30,31}. A large number of ions are moved in six-dimensional phase space, under the influence of the electric field arising from the self-consistently calculated potential ϕ , plus an optional force \mathbf{D} , to be explained in the next subsection:

$$m_i \frac{d\mathbf{v}}{dt} = -Ze\nabla\phi + \mathbf{D}. \quad (2)$$

The potential is represented on a cellular grid and satisfies

$$\nabla^2\phi = \frac{e}{\epsilon_0}(Zn_i - n_e). \quad (3)$$

The ion density (n_i) is determined by depositing the individual ions onto the grid (using Cloud in Cell³² particle shape) and the electron density is assumed to be governed by a thermal Boltzmann factor

$$n_e = n_{e\infty} \exp(e\phi/T_e). \quad (4)$$

Thus the treatment can be considered “hybrid” particle in cell and does not need to resolve the electron plasma time-scale.

Ions fill a computational region across whose outer boundary they leave or enter. Those entering are injected in accordance with the distribution function presumed for the external, uniform, plasma. The grain is represented by a fixed-potential sphere embedded in the computational region. It absorbs ions that strike its surface, but it does not emit any ions.

The conditions on potential at the outer computational boundary are chosen to represent most conveniently a potential decaying to zero at infinity ($d \ln \phi / d \ln r = -1$). Trials show that the precise choice of distant boundary condition does not affect the drag force.

The majority of the calculations here are carried out with the SCEPTIC code^{30,31}, which uses a spherical cell-grid conformal with the grain surface. The radial grid is uniform, which means that the cell-volume is proportional to the square of the radius (r). Up to 400 radial cells are used, depending on the domain size required to provide a converged result. The domain must typically be at least $\sim 2\lambda_{De}$ in radius to give accurate forces. Angular cells are equally spaced in $\cos \theta$ where θ is the positional angle with respect to the drift direction \mathbf{z} ; 100 angular cells are used. The potential is presumed 2-dimensional, independent of the azimuthal angle. The resulting cell size is much smaller than the Debye length, and sufficient to resolve the potential variation to an accuracy of a few percent. Up to 32 million ions are advanced for up to 4000 steps. A substantial fraction of those steps are in steady state and so can be averaged-over to improve statistics.

Some comparison calculations are made with the COPTIC code²⁵ to verify computational accuracy, confirm that domain size and shape are not substantially affecting the results, and explore extended wakes. COPTIC uses a cartesian grid but can accommodate oblique curved surfaces of embedded objects³³, such as the spherical grain that is used.

In either code, the force on the grain is calculated by accounting for the total momentum flux transferred by ions, electron pressure, and Maxwell stress inward across spherical surfaces containing the grain¹². The volumetric collisional momentum loss to neutrals within the sphere¹⁹ is subtracted and what remains is the total momentum transfer (rate) to the grain, i.e. the drag force on it. The fact that in steady state the momentum transfer is independent of the radius of the measurement sphere allows one to establish good convergence of the calculations by measuring at a number of different radii and observing equal results.

Because we are interested in quite large ratios of Debye length, λ_{De} , (which constrains minimum domain size) to grain radius, r_p , (which constrains maximum grid spacing at the grain) we are challenged in terms of computational capacity, and content ourselves with

overall uncertainty (both noise and spatial resolution error) of force measurement of up to approximately 5% (but usually smaller) plus an absolute uncertainty of roughly $2r_p^2 n_{e\infty} T_e$.

B. Collisions and Distributions

Charge-exchange collisions of ions with neutrals are represented in the code as a replacement of the ion velocity with a new velocity drawn randomly from the neutral velocity distribution. The simulations here use a collision frequency that is independent of velocity (equivalent to a BGK collision operator). Although not a perfect representation of the actual collision cross-section, this is sufficient to demonstrate the important new physics.

The nature of the collisions and the cause of the ion drift determine the self-consistent background distribution. The simplest case is when the ion drift is a reflection just of a neutral drift. In that case, which incidentally is equivalent by Galilean transformation to studying a grain moving through a stationary plasma, the ion velocity distribution in the unperturbed uniform plasma is simply equal to the neutral velocity distribution — which is the birth distribution of the ions after collisions. The extra force \mathbf{D} is then zero.

The opposite limit is when neutrals are (on average) stationary and the ion drift is driven by a uniform force field \mathbf{D} . The nature of this force field is generally unimportant for the calculations (except possibly in respect of the boundary conditions at the grain surface). It is usually thought to be a background electric field, but could theoretically equally well be gravity or some other unspecified force. It is important that the Boltzmann factor for electrons not take account of any potential gradient that is responsible for this driving force field \mathbf{D} because otherwise the solution of the system in the absence of a perturbing grain would not be uniform. That is why it is convenient to separate it out from the potential arising because of the grain: ϕ .

Intermediate cases are possible where the drift is partly driven by \mathbf{D} and partly by neutral drift. Their background ion distribution can then be represented by a shift of the collisional distribution. However, we present no simulation of such intermediate cases here. Different assumptions about collision cross-section dependence upon velocity lead to somewhat different distribution shape²⁰, they share many of the same features.

The solution of the ion Boltzmann equation for the unperturbed background plasma when the neutrals are Maxwellian has two very different forms, corresponding to shifted or

stationary neutrals. We call these the *shift* distribution ($\mathbf{D} = 0$) and the *drift* distribution ($\mathbf{D} \neq 0$) respectively. The shift ion distribution is simply equal to the neutral distribution: a shifted Maxwellian [$\exp(-m_i\{v - v_f\}^2/2T_n)$]. (The ion temperature can then be considered simply equal to the neutral temperature $T_i = T_n$ and we will not hereafter draw any distinction between T_i and T_n).

By contrast, in the absence of neutral shift, the drift solution of the Boltzmann equation for the ions gives a distribution that is the convolution of a stationary Maxwellian [$\exp(-m_i v^2/2T_n)$] with a half-exponential function representing the Poisson collision statistics [$\exp(-v_z/v_f)$ for $v_z > 0$, z being the direction of \mathbf{D}]. The resulting ion distribution can be expressed analytically as¹⁹:

$$f_i(\mathbf{v}) = \frac{n_i}{\pi v_{tn}^2} \frac{1}{2v_f} \exp\left(-\frac{v^2}{v_{tn}^2}\right) \operatorname{erfcx}\left(\frac{v_{tn}}{2v_f} - \frac{v_z}{v_{tn}}\right) \quad (5)$$

where $v_{tn} = \sqrt{2T_n/m_i}$ is the thermal speed and $\operatorname{erfcx}(x) \equiv \exp(x^2)\operatorname{erfc}(x)$. Notice that this form does not depend upon the actual value of the collision frequency ν_c or \mathbf{D} , only the mean ion velocity v_f and the thermal speed. Of course there is a definite relationship,

$$v_f = \frac{D}{m_i \nu_c}, \quad (6)$$

between \mathbf{D} and ν_c . Examples of the shifted Maxwellian distribution and the drift distribution are shown in Fig. 1. When $v_f \gg v_{tn}$ the ion distribution in the direction $\hat{\mathbf{z}}$,

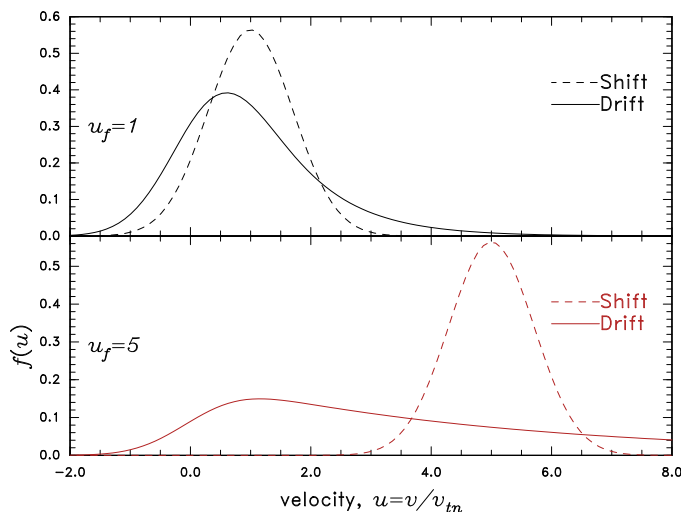


FIG. 1. Shift (shifted Maxwellian) and Drift (eq. 5) ion distributions for two values of the flow velocity, plotted versus velocity u , normalized to the neutral thermal velocity.

$f_z(v_z) = \int \int f_i dv_x dv_y$ is approximately a half-exponential $f_z(v_z) \approx n_i \exp(-v_z/v_f)/v_f$ for $v_z > 0$. An important feature is that its magnitude at small v is just n_i/v_f , inversely proportional to v_f , rather than falling rapidly to zero as it does for a shifted Maxwellian. This feature is common to any **D**-driven drift distribution, not just to the constant- ν approximation used here.

C. Yukawa drag force

It is helpful to compare the PIC calculations at low collisionality, with estimates based upon previously published momentum-transfer cross-sections calculated from orbits in Yukawa form potentials $\phi = Q \exp(-r/\lambda)/(4\pi\epsilon_0 r)$. Writing $\beta = b_{90}/\lambda = ZeQ/(4\pi\epsilon_0 m_i v^2 \lambda)$, a fit to the point-charge cross-section in the low-beta region $\beta < 1$, has been given as³⁴

$$\sigma_1 = \pi\lambda^2\beta^2 4 \ln(1 + 1/\beta) = \pi b_{90}^2 4 \ln(1 + 1/\beta), \quad (7)$$

In the limit of low β these become the classic cut-off Coulomb drag. In the high-beta region, $\beta \gg 1$, an asymptotic form is³⁴

$$\sigma_2 = \pi\lambda^2 0.8[\ln^2 \beta + 2 \ln \beta + 2.5]. \quad (8)$$

Although not perfect near $\beta = 8$, a reasonable fit to the Yukawa cross-section values, valid over the entire range, and having the correct limits, is to use for the combined cross-section, σ_y , a weighted sum of inverses thus:

$$\sigma_y^{-1} = [\sigma_1^{-1} + (0.15\beta)^2 \sigma_2^{-1}]/[1 + (0.15\beta)^2]. \quad (9)$$

To obtain the total drag force on a spherical grain of finite radius r_p , it has been shown^{9,13,15} that a good prescription is to change the form of the logarithm term in eq. (7) to

$$\ln \Lambda = \ln \left(\frac{b_{90} + \lambda}{b_{90} + r_p} \right) = \ln \left(\frac{\beta + 1}{\beta + r_p/\lambda} \right) \quad (10)$$

and add the momentum transfer by direct collection of those ions whose impact parameter is smaller than the OML critical impact parameter

$$b_c = r_p \sqrt{1 + e|\phi_p|2/m_i v^2}, \quad (11)$$

so that the force (in the z -direction) from this Yukawa-potential treatment is³⁵

$$F_Y = F_o + F_c = \int (\sigma_y + \pi b_c^2) m_i v_z v f_i(\mathbf{v}) d^3v. \quad (12)$$

Because we have from our PIC codes convenient representations of f_i , we can evaluate this integral numerically when comparing the PIC evaluations of the force with the binary collision treatment. The comparison is then not affected by additional approximations. We note, however, that there are already both significant approximations in using a Yukawa form, and significant uncertainties as to what value of λ to adopt.

D. Shielding length

It is often presumed that the shielding length to be used in collisional calculations of ion drag force is given by the so called linearized shielding length for which

$$\lambda^{-2} = \lambda_{De}^{-2} + \lambda_{Di}^{-2}. \quad (13)$$

Because $\lambda_D^{-2} = (Z^2 e^2 n / \epsilon_0 T)$ and $T_i \ll T_e$, the ion Debye length generally dominates in this expression unless the effective ion temperature is enhanced by sonic-speed-level ion flows.

However a Yukawa form potential with this shielding length is the solution to a linear approximation $n_i/n_{i\infty} = 1 - Ze\phi/T_i$ which is totally unjustified when $b_{90}/\lambda \gtrsim 1$, i.e. in the nonlinear regime. Although some studies¹⁰ have indicated that a Yukawa potential profile with a shielding length like this may not be too far wrong, those studies used mono-energetic ions, which is obviously a serious misrepresentation of the likely ion distribution function even when the drift velocity is small. Actually there exist analytic expressions for the spherically symmetric ion density in the vicinity of an ion-attracting probe in a stationary Maxwellian plasma³⁶. When intermediate energy barriers are ignored they reduce in the (applicable) limit $\lambda/r_p, |Ze\phi|/T_i \gg 1$ to

$$n_i = n_{i\infty} \sqrt{-4Ze\phi/\pi T_i}. \quad (14)$$

In other words, the ion-density rises proportional to the square root of $|\phi|$, not proportional to $|\phi|$. We will show that the nonlinear eq. (14) agrees reasonably well with the ion density that SCEPTIC finds.

Unfortunately no ready analytic expression is available to solve the nonlinear Poisson equation that then arises. And numerical solutions show poor resemblance to the Yukawa

form. However, a simple cut-off approximation can provide an appropriate scaling when $\lambda \gg r_p$ and ions dominate shielding, as follows. Suppose that the ion density is given by eq. (14). Suppose also that the dominant radial dependence of ϕ is the $1/r$ Coulombic variation, but only out to a cutoff radius. Take that cutoff radius r_c to be the place where the total ion charge within it is equal to $-Q/2$, so as to shield half the grain field. Then one can readily solve for r_c and find

$$r_c = \left(\frac{|Q|e}{4\pi\epsilon_0 T_e r_p} \right)^{\frac{1}{5}} \left(\frac{5\sqrt{\pi}}{8} \right)^{\frac{2}{5}} \left(\frac{r_p T_i}{\lambda_{De} T_e} \right)^{\frac{1}{5}} \lambda_{De} \approx 1.2 \left(\frac{r_p T_i}{\lambda_{De} T_e} \right)^{\frac{1}{5}} \lambda_{De}, \quad (15)$$

where the second form takes the grain potential to be $-2T_e/e$. Applying this scaling to a Yukawa cross-section is purely heuristic, but it gives a significantly longer shielding length. Table I illustrates the values of nonlinear shielding length, when $T_e/T_i = 100$. The corresponding linear values are all $\lambda/\lambda_{De} = 0.1$, $\lambda/r_p = 0.1\lambda_{De}/r_p$.

	$\lambda_{De}/r_p :$	10	20	50	100	200
NonLinear	r_c/λ_{De} (eq 15)	0.30	0.26	0.22	0.19	0.17
	r_c/r_p	3.0	5.2	10.9	19	33

TABLE I. Nonlinear shielding lengths.

Of course, an overall ion flow increases the effective shielding length even more, by reducing ion shielding through increased ion energy. For a shift distribution, it was found¹³ that appropriate shielding was obtained at substantial v_f using an almost-linear form

$$\lambda_\ell^2 = r_p^2 + \lambda_{De}^2/[1 + ZT_e/(T_i + \mathcal{E})], \quad (16)$$

where

$$\mathcal{E} = \mathcal{E}_s = 0.5m_i v_f^2 \left[1 + |v_f/0.4c_s|^3 \right] \quad (17)$$

represents the effects of flow.³⁷

We find the nonlinearity at low v_f is accommodated better by using r_c rather than λ_ℓ for the shielding length. A plausible and preferable nonlinear interpolation instead of eq. (16) is

$$\lambda^{-2} = \lambda_{De}^{-2} + (r_c^2 + \lambda_{De}^2 \mathcal{E}/T_e)^{-1}. \quad (18)$$

However, for drift distribution, the decrease in shielding with flow is anticipated to be predominantly by reducing the density of the low-velocity ion component proportional to

n_i/v_f . On this basis, the effective ion Debye length for shielding when $v_f \gg v_{ti}$ is obtained by replacing n_i (in $\lambda_{Di} = \sqrt{\epsilon_0 T_i / Z^2 e^2 n_i}$) by $n_i v_{ti} / v_f$, which is equivalent to adopting

$$\mathcal{E} = \mathcal{E}_d = T_e \sqrt{T_i / Z T_e} v_f / c_s, \quad (19)$$

in which the drift effect enters linearly in v_f rather than quadratically as in \mathcal{E}_s . The precise coefficient of v_f in eq. (19) is of course uncertain, but taking this simple one gives good results, when substituted into eq. (18), as we shall see.

E. Collection force expressions

For future use, it is convenient to have closed form expressions for the drag force eq. (12) that are easy to evaluate without having to do integrals. We present these here and in the next subsection.

The b_c^2 term of eq. (12) is from direct ion collection. It does not depend upon the shielding form in the OML limit. For a shifted Maxwellian distribution, it can be integrated directly to yield¹²:

$$F_{cs}(u_f) = n_i r_p^2 T_i \sqrt{\pi} \left\{ u_f (2u_f^2 + 1 + 2\chi) e^{-u_f^2} + \left[4u_f^4 + 4u_f^2 - 1 - 2(1 - 2u_f^2)\chi \right] \frac{\sqrt{\pi}}{2} \text{erf}(u_f) \right\} / u_f^2, \quad (20)$$

where $u \equiv v/v_{ti}$ denotes velocity normalized to ion thermal velocity and $\chi \equiv -Ze\phi_p/T_i$ is potential normalized to ion temperature.

To develop analytic expressions for the *drift* distribution, we recall that the drift distribution function can be written as the convolution of the Maxwellian (neutral) distribution with a half-exponential:

$$f(\mathbf{v}) = \frac{1}{u_f} \int_0^\infty \frac{n_i}{v_{ti}^3 \pi^{3/2}} e^{-(\mathbf{u}-s\hat{\mathbf{z}})^2} e^{-s/u_f} ds. \quad (21)$$

Since we have the closed form expression (20) for the collection force of a shifted Maxwellian distribution ($e^{-(\mathbf{u}-s\hat{\mathbf{z}})^2}$) already, we can therefore write immediately the drift distribution collection force as

$$F_{cd}(u_f) = \frac{1}{u_f} \int_0^\infty F_{cs}(s) e^{-s/u_f} ds. \quad (22)$$

Unfortunately eq. (20) does not lead to an integral that can conveniently be evaluated in eq. (22). However, an accurate ($\sim 2\%$) approximation to eq. (20) is

$$F_{cs}(u_f) = n_i T_i r_p^2 2\pi \left\{ u_f^2 + (1 + \chi) [1 - (1 + bu_f) e^{-au_f}] \right\} \quad (23)$$

where $b = 0.8$ and

$$a = b + \frac{(16 + 8\chi)}{6\sqrt{\pi}(1 + \chi)}. \quad (24)$$

The basis of this approximation is that for large u_f the exponential term is negligible and the remainder agrees with the asymptotic limit of eq. (20). At $u_f \rightarrow 0$, the form of a is chosen to give the correct linear dependence. And finally b is chosen ad hoc to improve the fit in the intermediate- u region. Fig. 2 shows that eqs. (23) and (20) are practically indistinguishable.

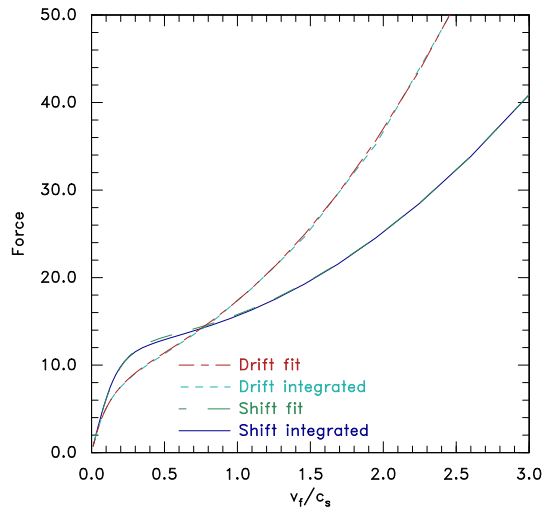


FIG. 2. Direct ion collection force analytic fits, eqs. (23) and (25) compared with numerical integration. $\chi = 200$.

Substituting eq. (23) with argument s in place of u_f , into eq. (22) gives an integral that can be evaluated as the following elementary expression:

$$F_{cd}(u_f) = n_i r_p^2 T_i 2\pi \left[2u_f^2 + (1 + \chi) \frac{(a - b)u_f + (au_f)^2}{(1 + au_f)^2} \right], \quad (25)$$

which is again indistinguishable from the numerically integrated result.

Equations (23) and (25) provide accurate and easily evaluated expressions for the direct collection ion force with shift and drift distributions respectively, but of course only when the actual level of collisionality is negligible. Notice that the u_f^2 term, dominant at large flow, is twice as large for the drift distribution as for the shift distribution.

F. Orbital Drag Force Expressions

The orbital part of the collisionless ion drag can be expressed as¹³

$$F_o = n_e T_e r_p^2 \left(\frac{Ze\phi_p}{T_e} \right)^2 \frac{T_e}{T_i} 4\pi G(u_f) \ln \Lambda, \quad (26)$$

which we will show compares favorably with the computational results.

For the *shift* distribution the function $G(u_f)$ is simply the Chandrasekhar function

$$G_s(u) \equiv \left[\text{erf}(u) - 2ue^{-u^2}/\sqrt{\pi} \right] / (2u^2). \quad (27)$$

The logarithm is written using the almost linear screening length, eq. (16), as

$$\ln \Lambda_s = \ln \left(\frac{b_{90} + \lambda_\ell}{b_{90} + r_p} \right), \quad (28)$$

and

$$b_{90s} = Ze\phi_p / (2T_i + \mathcal{E}_s), \quad (29)$$

where \mathcal{E}_s is given by eq. (17). In effect, this is a slightly adjusted form of the fit given in¹³.

For the *drift* case, because the relevant integrals cannot be performed analytically in the nonlinear regime, ad hoc approximations are used, putting

$$G_d(u) = u / (2.66 + 1.82u^2), \quad (30)$$

$$\ln \Lambda_d = \ln \left(\frac{b_{90d} + \lambda}{b_{90d} + 1.5r_p} \right), \quad (31)$$

and

$$b_{90d} = Ze\phi_p / [T_i + \sqrt{100T_i T_e r_p / \lambda_{De}} v_f^2 / (c_s^2 + 2.5v_f^2)]. \quad (32)$$

These are physically motivated and chosen to fit the numerical integrations, but are not known to be accurate outside the range $10 \leq \lambda_{De}/r_p \leq 200$ or for other temperature ratios.

The total drag force, $F_c + F_o$, is used in section III B to compare with the drag forces SCEPTIC finds.

III. ION VELOCITY DISTRIBUTION EFFECTS

A. Plasma Profiles

It is well established that in low collisionality, low T_i/T_e , approximately sound-speed flows the presence of a negatively charged particle produces an oscillatory wake. Although non-linearity strongly suppresses the magnitude of the wake potential it does not much change

its form. However, non-linear (and in fact most linear) calculations of wake structure thus far have used shifted Maxwellian ion distribution. An example is illustrated in Fig. 3(a), calculated with the COPTIC code, and in this display averaged over azimuthal angle and over 1000 timesteps. The first and most dramatic effect of considering collisions is the replacement

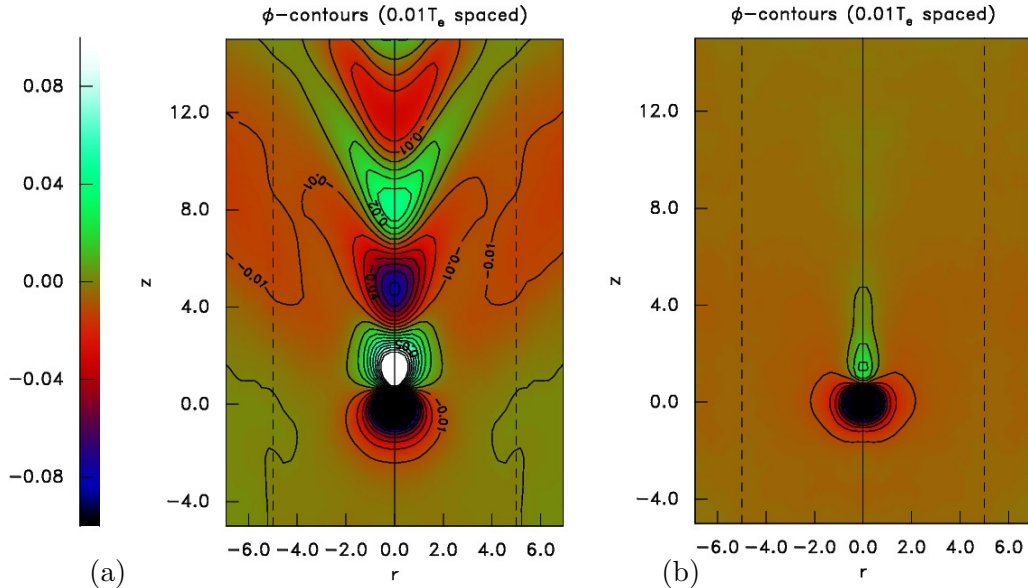


FIG. 3. Wake potential contours $e\phi/T_e$ for $v_f/c_s = 1$, $r_p = 0.1\lambda_{De}$, $\phi_p = -2T_e/e$, $T_e/T_i = 100$, negligible collisionality, calculated by COPTIC. Two contrasting background ion distributions: (a) shifted Maxwellian; (b) drift distribution eq. (5). Lengths are here scaled to λ_{De} and the grain is at the origin.

of the shifted Maxwellian with the drift distribution eq. (5). Fig. 3(b) shows the effect of that replacement. The actual collisional level is completely negligible ($\nu_c r_p/c_s = 10^{-4}$) for all the results of this section. The two calculations can be considered collisionless but simply with different background ion distributions. The drift distribution (b) completely wipes out the wake oscillations, greatly reduces the height of the trailing peak in the potential from about 0.2 to 0.03 T_e/e , and elongates the peak further downstream.

Both of these cases exhibit large ion density enhancements (about 10 times background) trailing the grain (i.e. at small positive z), as illustrated in Fig. 4. These are snapshots of instantaneous density slices through the three-dimensional domain, which therefore give an indication of the statistical fluctuations in the density. Note that the non-uniform grid has much smaller spacing near the origin to accommodate the fine potential structure there. Because the grid spacing is smaller than λ_{De} , the potential fluctuations are smaller than the

density fluctuations, even before the averaging performed for Fig. 3. The predominant difference between the two density profiles is that the shift distribution (a) has negligible density perturbation upstream of the grain whereas the drift distribution (b) gives, in addition to the high peak immediately trailing the grain, a “halo” of enhanced ion density around the grain, including in the upstream direction, and a somewhat longer ridge in the downstream direction. The shift distribution density drops below the background level at the down-

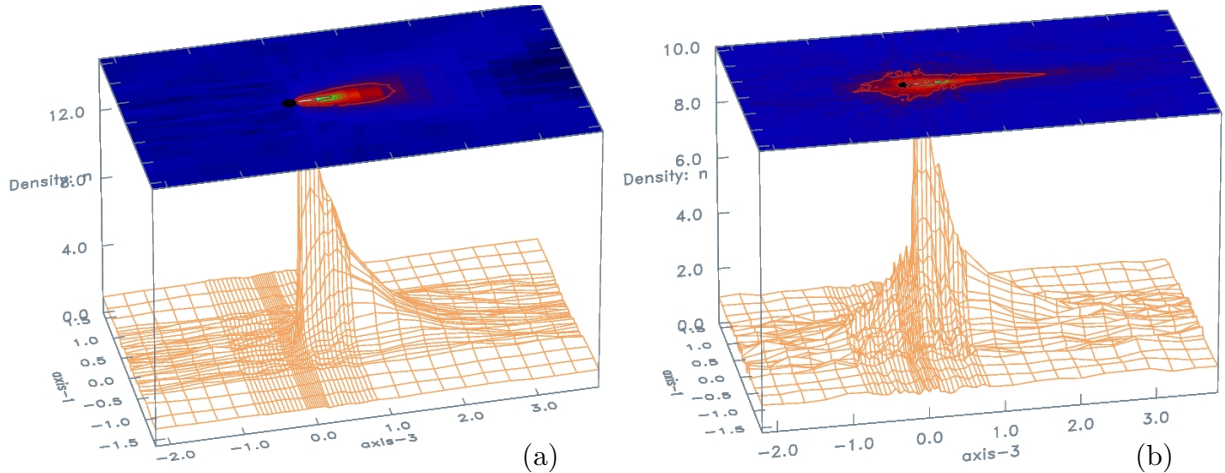


FIG. 4. Spatial profiles of ion density (scaled to the background) for the simulations in Fig. 3. Shift (a), and Drift (b) distributions. (A restricted region of the calculation is plotted. Axis-3 is z , the flow direction. Lengths are scaled to λ_{De} .)

stream edge of the region plotted in Fig. 4(a), corresponding to the negative oscillation in potential. The drift distribution (b) does not have this overshoot in density.

The “halo” of ion shielding arises predominantly from the lower-velocity component of the ion distribution, which is absent from the shift distribution. Prior simulations of the shift distribution case¹³ showed that the upstream shielding cloud is present for shift velocities lower than approximately $0.5c_s$, and that the transition in shielding is quite abrupt partly because of potential asymmetries. It is therefore of interest to understand better the ion shielding by ions of low velocity (which are always present in the drift distribution) and at low drift velocity (which causes slow ions for the shift distribution).

Fig. 5 shows a contour plot in the r, z plane of the ion density found by SCEPTIC for $v_f = 0.2c_s$ with drift ion-distribution. Here $\lambda_{De} = 50$ (lengths scaled to r_p) and only the inner quarter radius of a total domain $r = 100$ is plotted. There is residual asymmetry in

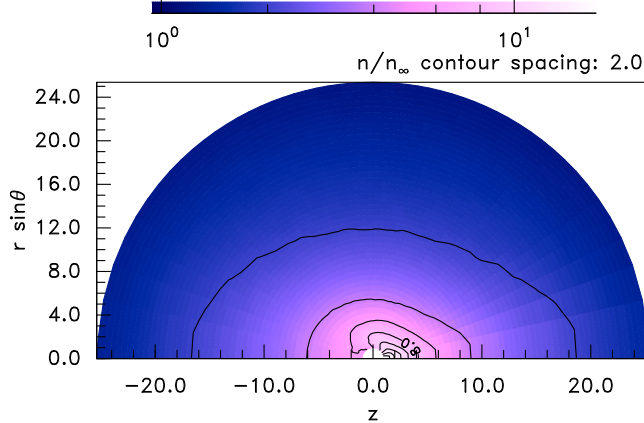


FIG. 5. Color contours of density calculated by SCEPTIC. $\lambda_{De} = 50r_p$, $v_f = 0.2c_s$ drift distribution. Lengths are scaled to r_p . Flow is in the $+z$ direction.

the ion density, consisting of elongation of the shielding ion cloud both downstream and up, giving both dipole and quadrupole potential perturbations. In this plot, averaging over 1000 steps has suppressed the cell-to-cell statistical noise level (arising because the number of ions per cell on this 200×100 uniform in r and $\cos\theta$ spherical grid is only of order unity in the smallest cells near $r = 1$).

For sufficiently low ion drift (or shift) the density is approximately spherically symmetric. In Fig. 6 is shown the angle-averaged total ion density versus radius and that part of the density attributable to trapped ions. The solid line is for a drift case with $v_f = 0.05c_s$, but the results are essentially the same for a shift distribution (shown as dotted line) at this low v_f . For comparison we also show the results of the analytic approximations for the variation of density with potential (ϕ , taken from the angle-average of the simulation). The nonlinear expression, $n_i/n_{i\infty} = \sqrt{1 - 4Ze\phi/\pi T_i}$, regarded as a suitable extension of eq. (14), agrees remarkably well with the simulation; the linearized expression, $n_i/n_{i\infty} = 1 - Ze\phi/T_i$ is too large by a factor reaching greater than 10.

As the plasma flow is increased, the ion shielding becomes asymmetric, of course, but also this angle-averaged ion density shows changes for $v_f \gtrsim 0.2c_s$. Fig. 7 shows that by the time $v_f = 1.c_s$, the drift ion-distribution gives rise to shielding density approximately a factor of two less than at low v_f , and correspondingly longer shielding length. However, the shift distribution shows much greater ion density suppression, so that ions are hardly shielding the grain at all. There is thus a major difference in ion shielding between drift and shift

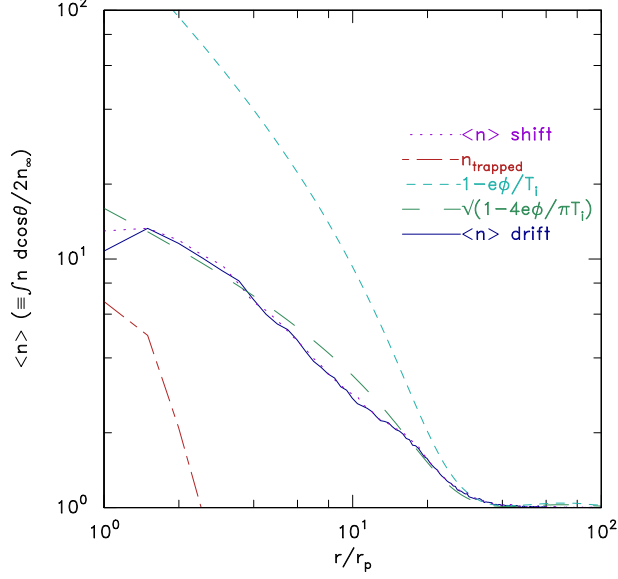


FIG. 6. The angle-averaged ion density (solid line) for a SCEPTIC calculation with $\lambda_{De} = 50r_p$, $v_f = 0.05c_s$ (drift distribution) compared with nonlinear and linear analytic expressions (dashed lines). Also shown (dotted) is the shift distribution density, virtually the same. Particles trapped in the potential well but with sufficient angular momentum to avoid collection are a small fraction except very close to the grain.

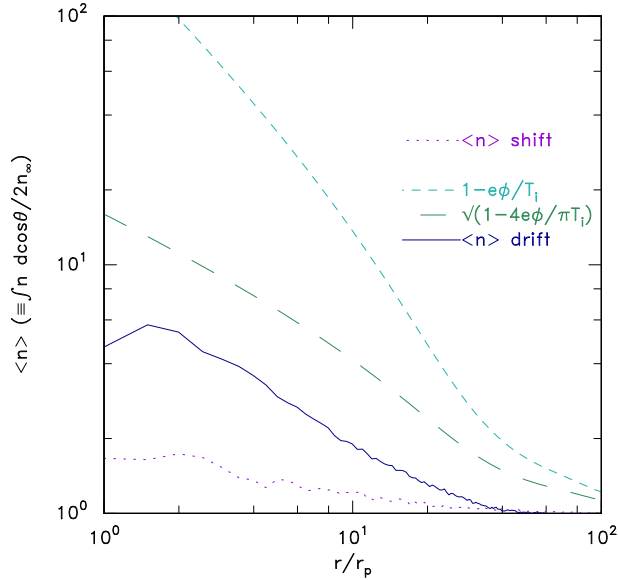


FIG. 7. The angle-averaged ion density (solid line) for a SCEPTIC calculation with $\lambda_{De} = 50r_p$, but sonic flow $v_f = 1.c_s$ with drift and shift distributions. The shielding length is much longer and the density no longer agrees with the nonlinear symmetric expression.

distributions, when v_f is substantial.

B. Collisionless Drag forces

We now document the drag force at negligible collisionality level for the shift and drift distributions calculated using SCEPTIC, and compare them with binary collision calculations using Yukawa cross-section, with the same ion distributions.

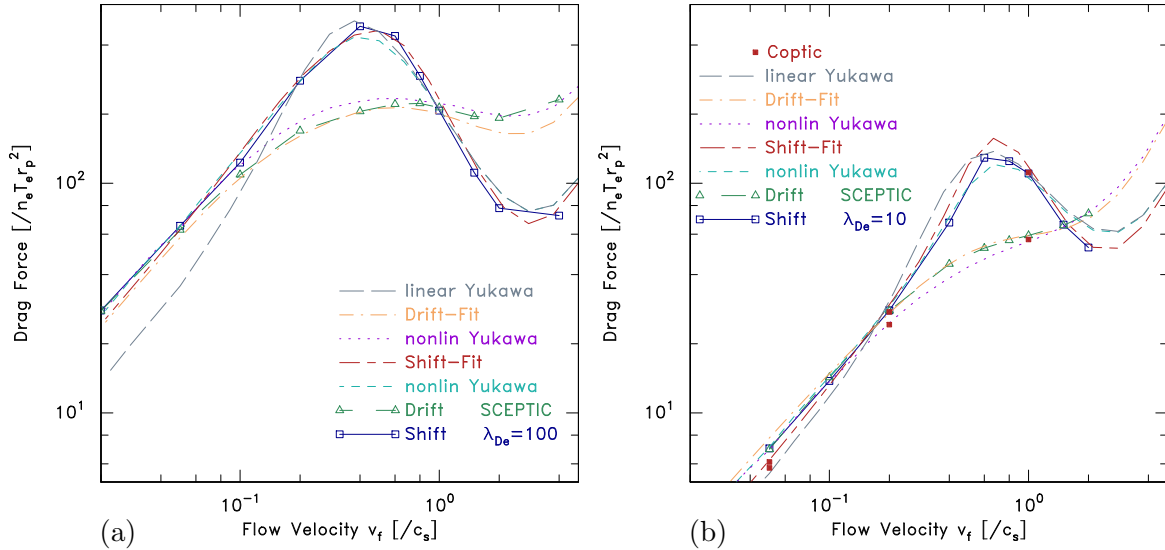


FIG. 8. Force as a function of ion flow velocity for shift ($v_n = v_f$) and drift ($v_n = 0$) distributions: (a) $\lambda_{De} = 100r_p$; (b) $\lambda_{De} = 10r_p$. Points are SCEPTIC calculations. Short dashed lines are the shift-distribution Yukawa cross-section collision numerically integrated using nonlinear shielding form (eqs. 17,18). Short-long dashes are the corresponding analytic Shift-Fit of section II F. Dotted and dot-dash lines are the same for the drift distribution (eqs. 19,18). Long dashes with short gaps is the shift Yukawa case using *linearized* shielding length corrected for flow (eqs. 17,16). In (b) some independent code verification cases from COPTIC are shown.

In Fig. 8(a) we see, first, that there is a dramatic difference in the drag force between the shift and drift distributions measured by SCEPTIC (points). They agree with each other only at very small flow velocity $v_f \lesssim 0.15c_s$, where the distributions become almost indistinguishable. For the drift distribution, drag is approximately constant from $v \sim 0.2c_s$ upward. The shifted Maxwellian, in contrast, has a strong peak at $v \sim 0.5$ more than twice as high, and then rolls rapidly off to approximately half the drift-distribution force

at $v = 2c_s$. Values derived from integrating eq. (12) using the best nonlinear analytic estimates (eqs. 15,17,18,19) of the shielding-length variation, and convenient fits (eq. 26 and following, subsection II F) are shown. They agree reasonably well with the corresponding SCEPTIC results. However, using instead the linearized shielding length (eq. 16) gives numerically integrated values that are nearly a factor of 2 too low at low flow velocity $v \lesssim 0.1c_s$). Fig. 8(b) shows a similar comparison for ten times shorter Debye length: $\lambda_{De} = 10$. Reasonable agreement is obtained with all analytic forms. The discrepancy arising from incorrect shielding length at low v_f is now mostly compensated by the term r_p in eq. (16) for the shift case. Shift and drift distribution force at $v_f/c_s = 0.05, 0.2, 1.0$ derived from the totally independent code COPTIC are plotted as filled boxes. They show agreement with SCEPTIC results within the probable uncertainty of both codes. The agreement of the Shift-Fit curve is somewhat fortuitous. It arises because the error induced by using the linear cross-section approximation eq. (7) (at β values beyond its applicability) is compensated by an opposite error from using linear shielding, λ_ℓ , eq. (16). Of course, that fit was initially developed using SCEPTIC results, so it is not surprising that it agrees with the current data.

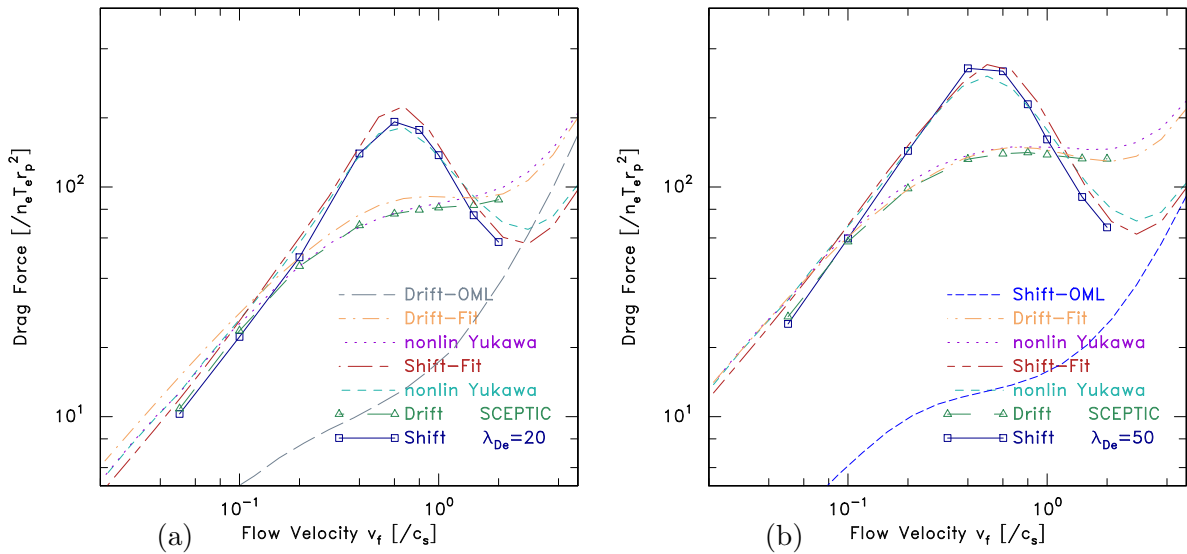


FIG. 9. Like Fig. 8 except that in (a) $\lambda_{De} = 20r_p$ and the OML direct collection drift-distribution component is shown; in (b) $\lambda_{De} = 50r_p$ and the shift-distribution OML component is shown.

Fig. 9 shows cases $\lambda_{De} = 20r_p$ and $\lambda_{De} = 50r_p$, in which the analytic agreement with SCEPTIC results is still quite good. We also show the direct collection ion component of

the forces, eqs. (23), (25), which is included in the forces of all the plots of these sections, and whose value is independent of λ_{De} . It plays a significant role, especially in the lower λ_{De} cases, and becomes dominant for all cases when $v_f \gtrsim 4c_s$.

These observations establish that it is possible to get collisionless drag force from a Yukawa-potential binary-collision treatment. However, it is accurate for fairly large λ_{De}/r_p only if the appropriate shielding length is used. The shielding length value used must be nonlinear (r_c) at low v_f , and the variation with v_f must account for the difference between shift and drift distributions.

IV. FINITE COLLISIONALITY DRAG FORCE

We now present a comprehensive documentation of the ion drag force calculated using SCEPTIC as a function of collisionality, Debye length, and flow velocity for the drift and shift cases. In all cases the grain potential is kept fixed at $-2T_e/e$. This might not be the floating potential, which will undoubtedly vary. However our intention is to focus on the drag force's intrinsic variation, and for that purpose it is better not to confuse the issue with another variable (ϕ_p). The leading dependence of drag is that it is $\propto \phi_p^2$ (see eq. 26).

Fig. 10 shows logarithmic plots of drag force variation with collision frequency ν_c expressed in units of c_s/r_p . We observe as follows.

(a) at low flow velocity, $v_f = 0.05c_s$, the force at low collisionality is constant, equal to the zero collisionality values already given, and the drift and shift cases are the same. As collisionality increases, the force rises to a maximum roughly a factor of 2 higher than the collisionless level. Near the maximum, the drift case force begins to rise above the shift case. Then as collisionality further increases, the forces begin to decrease reaching an asymptotic slope of approximately -1 ($F \propto 1/\nu_c$).

(b) at moderate flow velocity, $v_f = 0.2c_s$, at smaller λ_{De} similar behavior occurs. But at larger λ_{De} the forces are unequal at very low collisionality, with the shift case higher than the drift, consistent with the collisionless behavior given already. Beyond the peak of the force, the shift case crosses to below the drift case.

(c) at flow velocity $v_f = 0.6c_s$ approaching sonic, the shift case no longer shows any force increase with collisionality. Instead it stays almost constant until the high collisionality roll-off is reached. The drift case still has a peaked shape, but at large λ_{De} it occurs at lower ν_c

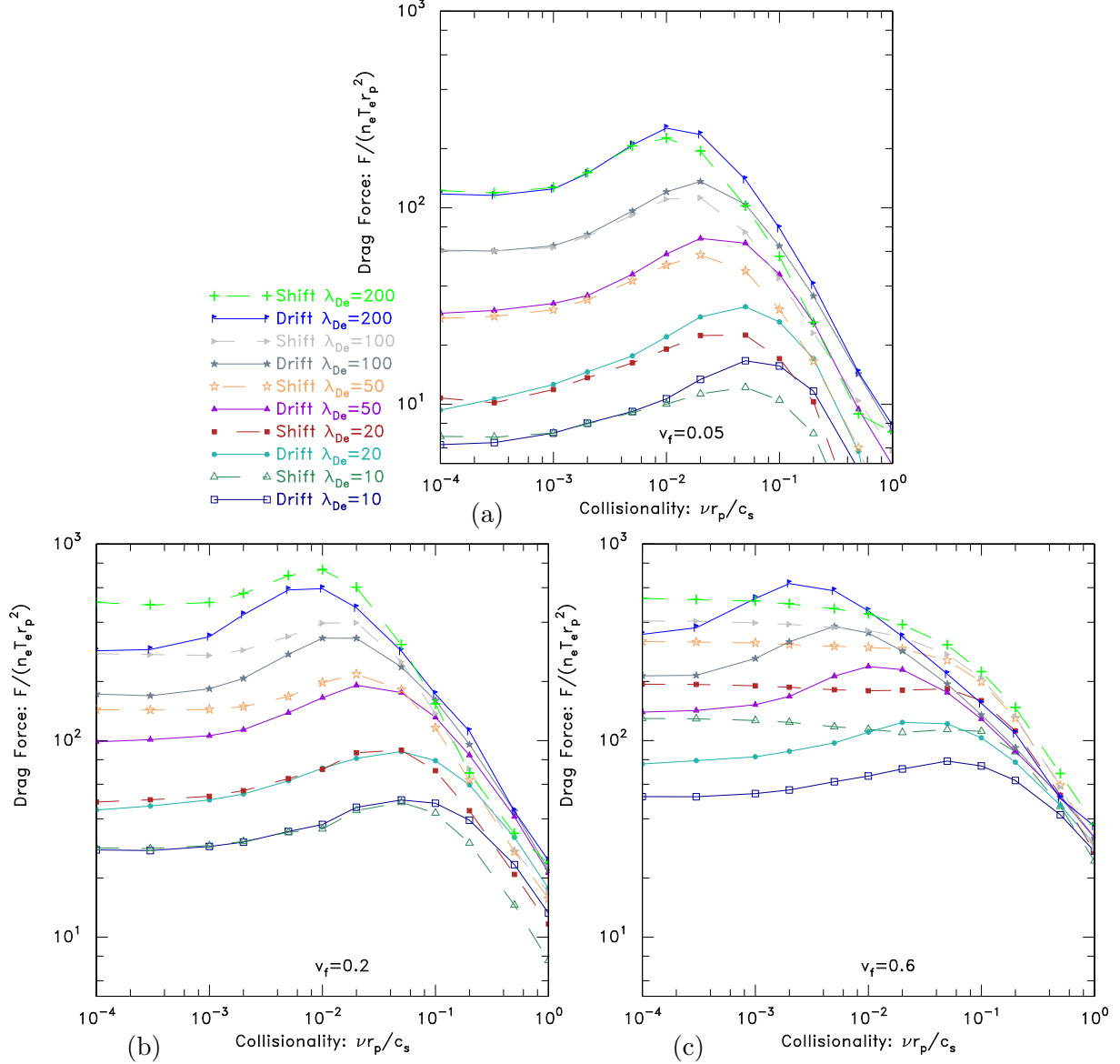


FIG. 10. Drag force in normalized units as a function of collisionality for drift velocity v_f equal to (a) 0.05, (b) 0.2, (c) 0.6 (times c_s). Five different values of Debye length (in units of r_p) are shown, each for the drift ($v_n = 0$) and the shift ($v_n = v_f$) case.

than for the lower flow velocity cases, and there is a substantial region where the force falls more slowly than $1/\nu_c$.

In all cases the force is greater for greater λ_{De} when other factors are equal.

In Fig. 11 is shown the drag force as a function of flow velocity. It is therefore a plot along an orthogonal axis of parameter space. Two values of collisionality are shown: $\nu_c = 10^{-4} c_s / r_p$, which is essentially collisionless, and $\nu_c = 10^{-2} c_s / r_p$ which is near the peak of the

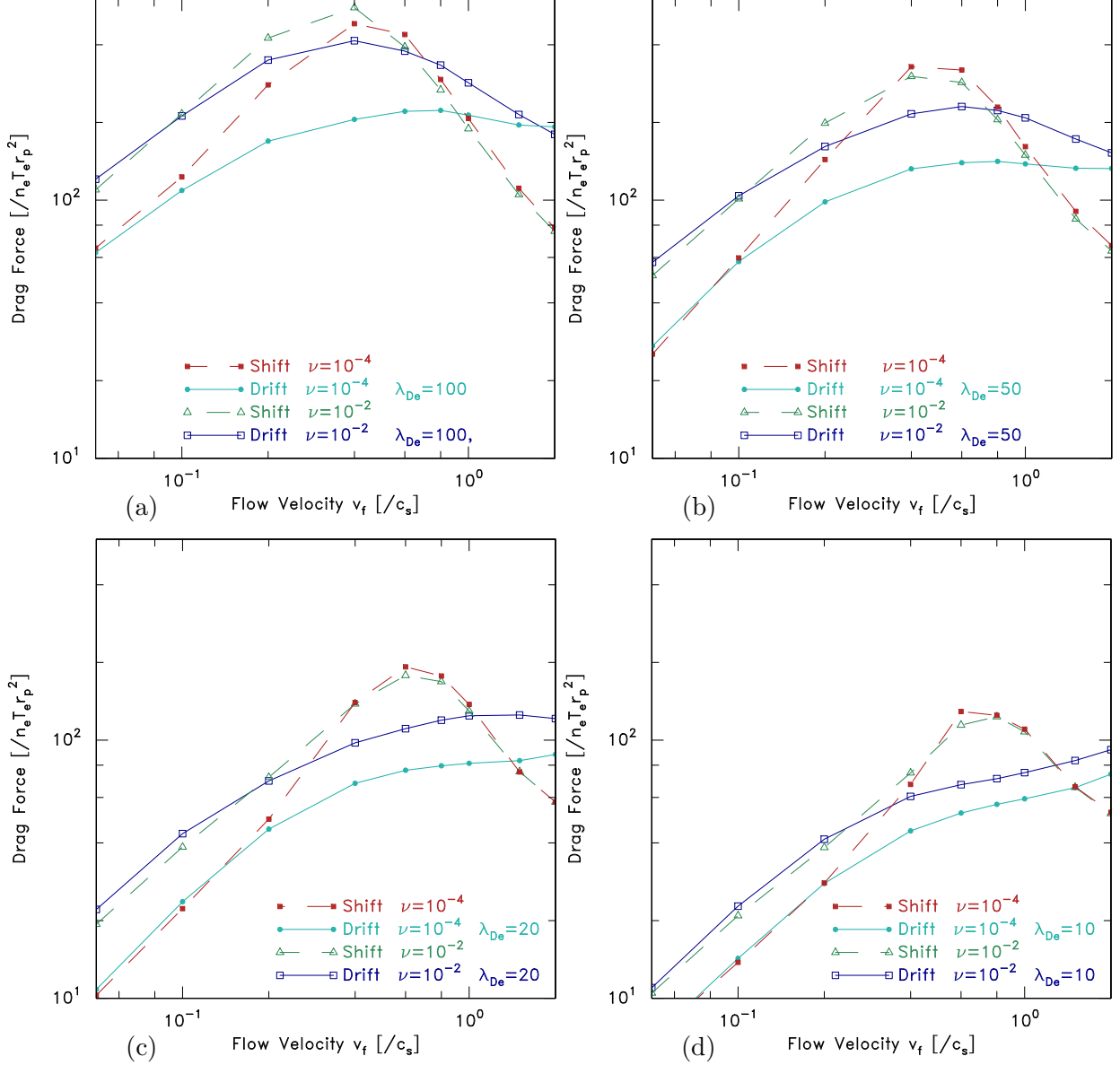


FIG. 11. Drag force as a function of flow velocity for values of the Debye length (in units of r_p) (a) 100 (b) 50 (c) 20 (d) 10. Two values of collisionality ν_c in units of c_s/r_p are shown, for the drift and shift cases. The $\nu_c = 10^{-4}$ cases are practically collisionless, while the $\nu_c = 10^{-2}$ cases are near the peak of the collisional force-enhancement.

force versus collisionality curves. We observe the following.

At low flow velocity the drift and shift curves are nearly, but not exactly the same at $\nu_c = 10^{-2} c_s/r_p$ and both are approximately a factor of 2 above the $\nu_c = 10^{-4} c_s/r_p$ collisionless values. The difference decreases somewhat as λ_{De} decreases. The shift case makes a quite rapid transition so that for $v_f \gtrsim 0.4 c_s$ there is no difference between the collisional and

collisionless forces. This transition is, of course, the difference between Figs. 10(b) and (c). The Drift case shows no such transition and the collisional force enhancement is maintained up to $v_f \sim 2c_s$ for $\lambda_{De} = 100$, and further for lower Debye length. The drift force is far from a $1/v_f$ asymptote for all velocities $v_f < 2c_s$.

To express systematically the modification of the drag force that arises from finite collisionality, it is best to use a definition of collisionality that is scaled to the size of the ion shielding cloud, rather than the grain radius: $\bar{\nu} = \nu_c r_c / c_s$. If we then divide the drag force by its collisionless value, we get a collisional *correction factor* $\bar{F} = F(\bar{\nu})/F(\bar{\nu} = 0)$ relative to the collisionless case.

Fig. 12 shows how this scaling reduces the data of Fig. 10 to approximately universal curves (different for different velocities) that vary little with Debye length. The curves can be fitted with a simple rational function:

$$\bar{F}(\bar{\nu}) = \frac{1 + a\bar{\nu}}{1 + b\bar{\nu} + c\bar{\nu}^2} \quad (33)$$

in which the coefficients are given by Table II.

Case	a	b	c
Drift	$(7 + 30v_f/c_s)$	$18v_f/c_s$	$0.5a$
Shift	5	$8v_f/c_s$	3.2

TABLE II. Coefficients for the shift and drift cases of eq. (33).

This fit is optimized for the larger Debye-length cases, which are the more immediately relevant to most experiments. It can be seen that at lower Debye length some deviation from universality is present. The accuracy of the fit may be judged from Fig. 13. However, the fit cannot be trusted for low flow velocities at collisionalities higher than $\bar{\nu} \approx 1$. There the force becomes very small and actually reverses sign.

V. DISCUSSION

The following qualitative discussion helps to explain the observed trends. It is based upon the observation that for the large temperature ratio plasmas under discussion, the plasma shielding of the grain charge is done mostly by ions. Until the collisionality becomes strong or the ion flow is fast enough that the electrons participate strongly in shielding, the

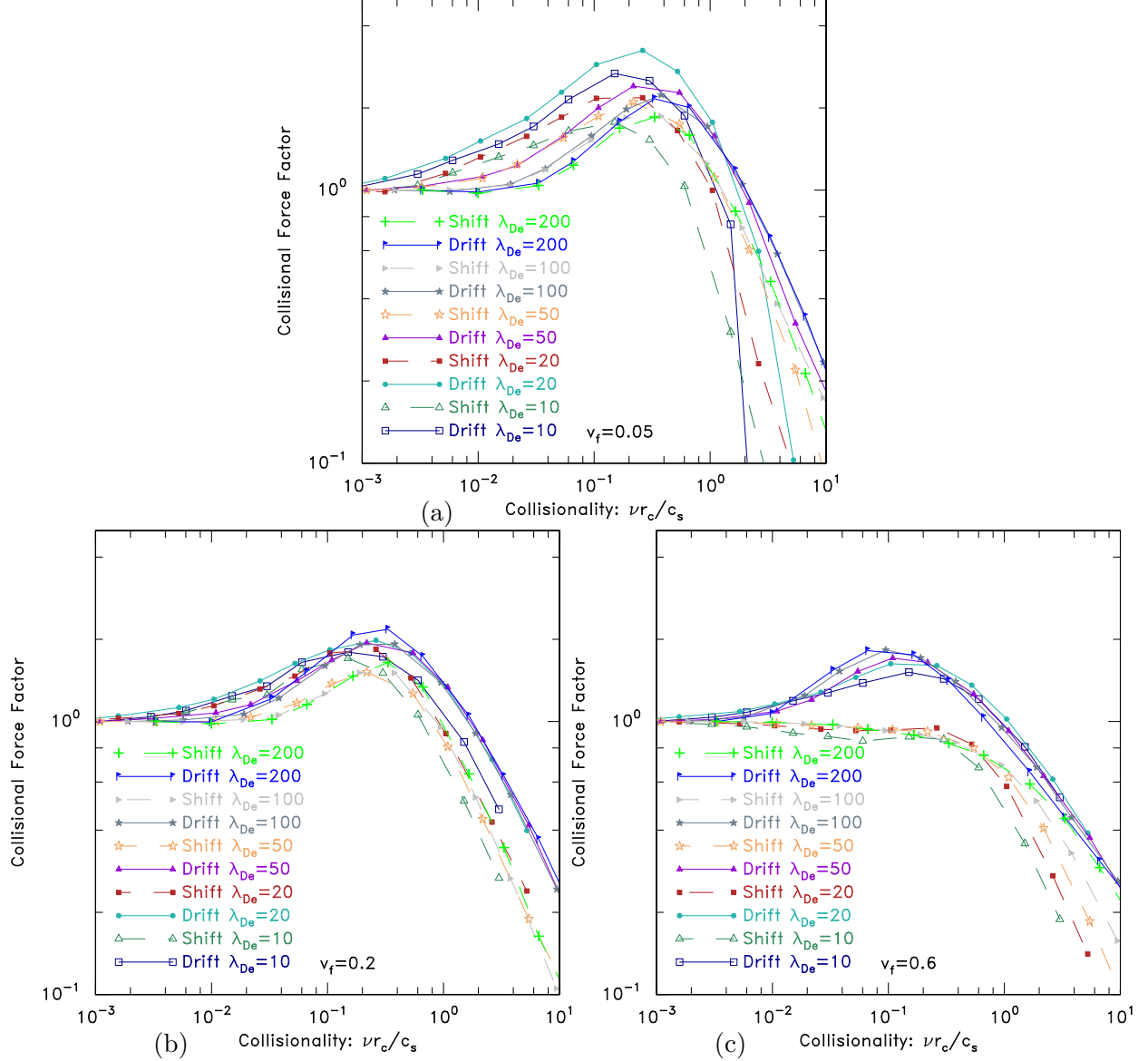


FIG. 12. The drag force divided by its collisionless value, i.e. \bar{F} , as a function of collisionality $\bar{\nu} = \nu_c r_c/c_s$ relative to the ion-cloud radius r_c , for drift velocity v_f equal to (a) 0.05, (b) 0.2, (c) 0.6 (times c_s). Five different values of Debye length (in units of r_p) are shown, each for the drift ($v_n = 0$) and the shift ($v_n = v_f$) case.

shielding cloud consists of a total charge of ions equal to minus the charge on the grain, regardless of shielding length. We call these resident ions. Let us first consider the shift distribution at small flow, $v_f/v_{tn} \lesssim 1$.

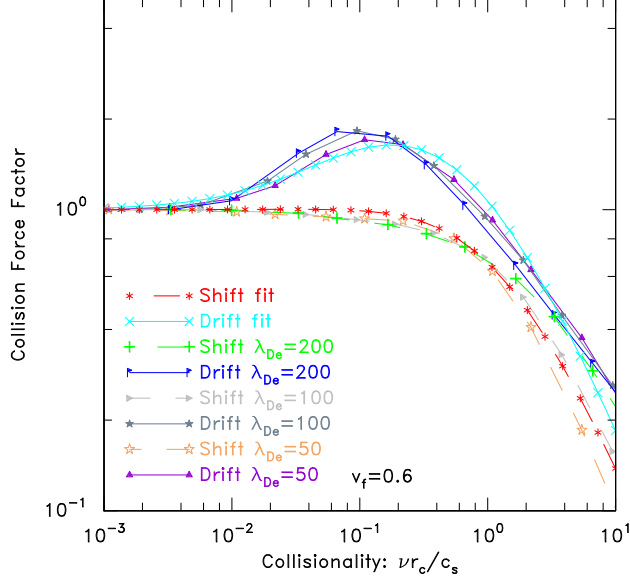


FIG. 13. Illustration of fit to collisional force factor, \bar{F} , from eq. (33), for the case $v_f = 0.6c_s$.

A. Collisionless Drag Scaling

Virtually all the ions that enter the shielding cloud and participate in drag have orbits with large scattering angle, because $b_{90} > \lambda$. Therefore on average they exit at a random angle with approximately zero directed momentum. They therefore lose on average approximately their incoming directed momentum which is transferred to the grain. This observation has been demonstrated numerically for Yukawa shielding¹⁴ and is part of the estimate of the (collisionless) Yukawa momentum cross-section at high β .

The residence time of the ions in the cloud is proportional to the shielding length (i.e. the radius of the cloud) because their speed is essentially independent of cloud size, and their residency orbit length is proportional to shielding length.

Therefore the collisionless drag force, which is the rate of momentum transfer from ions to grain, is proportional to the number of shielding ions divided by the residence time, and hence the number of shielding ions divided by the shielding length. When normalized by density $nT_e r_p^2$, a factor of λ_{De}^2 is introduced, which when divided by shielding length approximately proportional to λ gives a scaling of drag force $\propto \lambda$ in the collisionless limit. Note that λ is not exactly $\propto \lambda_{De}$ because of the nonlinearity of shielding length, so this is only an approximate scaling.

B. Effect of a small finite level of collisionality

Suppose the collision time is longer than the residence time.

Almost all collisions to resident ions produce an ion unable to escape the grain's potential well, because its prior velocity is replaced by a velocity v_i drawn from the shifted neutral distribution. If the shift is small (low v_f), then because the ion is on average resident at a place where $-2\phi/m_i v_i^2$ is > 1 , it is captured. Some such captured ions will have low enough angular momentum to be immediately directly collected by the grain. Actually, for smaller λ_{De} a quite large fraction of the collided ions experience this effect. The average momentum a directly collected ion has after its last collision before collection, is soon thereafter transferred to the grain. Any momentum it gains in the field prior to arrival at the grain is cancelled out by the force it exerts on the grain during its acceleration. Thus, only the birth momentum, mv_i , which has a directed mean mv_f , is gained net by the grain.

The birth momentum of a collision that does *not* lead to immediate collection is still *on average* transferred during the ion's trapped phase to the grain by electric force, provided the trapped ion makes at least one orbit. Therefore, when the collision time is longer than the orbit period, regardless of whether a collided ion is immediately collected or not, its birth momentum is transferred in a time of order one orbit to the grain.

Whether a resident ion is trapped or not, it still contributes to shielding, and is still subject to collisions that cause birth momentum transfer to the grain. The rate at which collisions are happening to resident ions is just their number, $N_i = -Q/Ze$, times the collision frequency ν_c . There is therefore an additional drag force, arising from collisions, approximately equal to

$$- Q\nu_c mv_f / Ze. \quad (34)$$

It is *independent* of shielding cloud size and proportional to collision frequency and flow velocity.

Prior to a collision, the resident ion has transferred some of its incoming momentum (or if it previously collided, its birth momentum) to the grain. The presumption, so far, is that provided the collision time is longer than the residence time, on average all of the incoming momentum has already been transferred, by the time a collision occurs. In the nonlinear regime under consideration, most resident orbits in a Yukawa potential in fact have greater than 180 degree scatterings, and many more than 360 degrees¹⁴. Since rare collisions occur

on average half way through the residency, approximately 180 degree residency implies on average 90 degree scattering prior to a collision, and hence full momentum transfer, justifying the presumption.

C. Collision time comparable to residence time

If the collision time becomes shorter than the time of scattering through 180 degrees, then the momentum transfer prior to the first collision will average less. However, in that case, multiple collisions will be important too, and more complicated considerations arise. At the threshold of onset of these complications, an ion has on average approximately one collision during a transit. That is, the collision time is equal to the residency time. If that is the case, then the drag will have been increased by a factor of approximately two, because a transiting ion will have transferred its incoming momentum plus one collision's worth of birth momentum (both of which are on average mv_f) to the grain. Therefore the collisional effects cannot increase the drag by more than approximately a factor of two before multiple collision effects have to be considered.

If the collision time is noticeably shorter than the orbit time, then: (1) The incoming momentum is not all transferred to the grain. (2) The birth momentum of each collision is also not all transferred to the grain. Collisions intervene during the momentum transfer process and transfer what remains to the neutrals instead.

D. Drift case

In the drift case at long collision time, what happens is that a collided ion is (re)born with zero average momentum. There is therefore no momentum transfer per se arising from collisions. However, all resident ions are instead acted upon by the accelerating drift force field $D = \nu_c mv_f$. Resident ions transfer essentially all of this momentum to the grain by virtue of the potential well electric field. So collisions introduce an additional drag force that is simply $N_i D = N_i \nu_c mv_f$. This is the same as the shift additional collisional force, eq. (34).

The collisional enhancement becomes comparable to the collisionless drag term (only) when the collision time becomes comparable to the residence time. When the collision time

is shorter than the residence time, not all the momentum gained from D is transferred to the grain. Therefore virtually the same argument applies to the Drift case as the shift case. The drag enhancement due to collisions cannot exceed approximately a factor of 2.

E. Large flow velocity

When v_f becomes $\gg v_{ti}$, there is a major difference between the drift and the shift case.

Drift ions are still born with the same, zero-average, velocity. There is essentially no difference in the argument above, the collisional force can be considered to be just the driving force field acting on the shielding cloud.

Shift ions, however, are born with an average velocity equal to the flow velocity. If this is large enough to exceed the potential-well escape velocity (from their birth position), then they *will not* transfer all their momentum to the grain, regardless of collisionality. Instead they will transfer only the momentum corresponding to their energy loss escaping the well, and this will be a small fraction once the birth energy substantially exceeds the (average) potential depth. This explains why the collisional force enhancement disappears for the shift case when $v_f \gtrsim 0.3c_s$ or a bit lower at higher λ_{De} . This is the velocity where the flow energy exceeds roughly $\phi_p/2\lambda$, and birth ions are no longer trapped.

F. Continuum Regime

When the collision time becomes substantially shorter than the orbit time, we begin to move into the continuum regime where collisions dominate. We find that the charge on the grain is no longer completely shielded. Residual Coulomb-like electric field is required to attract the ions from large distances into the potential well and eventually to be collected³⁸. In this regime the drag begins to fall off approximately inversely proportional to collisionality, but under some circumstances actually reverses sign. It has been demonstrated¹⁹ that SCEPTIC force calculations agree with analytic solutions to the continuum equations at high collisionality.

An unexpected new observation in the present data at intermediate and high collisionality is that at low flow velocity, the ion drag force for the drift case significantly exceeds the shift case. The SCEPTIC results show that drag in these cases arises from an enhancement of

the ion density downstream of the grain, caused by focusing of the ions as they flow past. The drag *difference* is observed in the simulations to be a result of the downstream density enhancement being greater for the drift case. The direct ion momentum collected by the grains in at low flow velocity (e.g. $v_f = 0.05c_s$) is actually a negative contribution to the drag, but until one is deep into the collisional regime the total drag is dominated by the electric field force that arises from the downstream density enhancement. The small ($\sim 10\%$) density asymmetry gives rise to an even smaller ($< 1\%$) potential deviation from spherical symmetry. Yet this is what is responsible for the drag; and the asymmetry magnitude is different for the drift and shift cases. We speculate that the density difference can be explained heuristically as arising from the combination of non-uniform accelerating field (approximately Coulomb field close to the grain) and finite Knudsen number (collision mean free path relative to scale size), which can be shown to lead to a difference in flow velocity between drift and shift cases.

VI. SUMMARY

The ion drag force on a spherical grain in a flowing collisional plasma has been calculated using the SCEPTIC and COPTIC particle in cell codes over a wide range of collisionality, flow velocity, and Debye length, for grain potential $-2T_e/e$ and temperature ratio $T_e/T_i = 100$. These self-consistent calculations take into account the fully non-linear behavior that arises with typical dusty plasma experiments because the ion ninety-degree impact-parameter length (sometimes called the Coulomb radius) is similar to or exceeds the Debye length.

For negligible collisionality, it is found that using the ion distribution function appropriate for *drift* driven by a force field makes a major difference compared with using a *shifted* Maxwellian in which the same ion flow arises from neutral background flow without a force field. In comparison with the more widely studied shifted Maxwellian case, the wake potential of the drift case is far smaller in magnitude and has no oscillations (regardless of collisionality). The low-collisionality drift-distribution drag force is up to a factor of two smaller than the shift-distribution force in the subsonic flow range ($0.2 < v_f/c_s < 1.$) and up to a factor of two larger for supersonic flow. These differences can be explained on the basis of approximating the ion interaction with the grain as being scattering in a Yukawa

potential. However, quantitative agreement is obtained only if the full nonlinearity not only of the scattering cross-section, but also of the shielding length is accounted for. Comprehensive analytic formulas representing the integrated forces, and verified in comparison with the simulations, are given³⁹.

Finite collisionality initially enhances the drag force, but only by up to a factor of ~ 2 relative to the negligible collisionality value. At flow velocities greater than $\sim 0.5c_s$, collisional drag enhancement occurs only for drift distributions, not shift distributions. As collisionality increases further, with collision frequency above $\sim 0.2c_s/r_c$, the drag force falls off approximately inversely with collisionality (but eventually reverses). Surprisingly, it is observed that at very low flow velocity, where the *collisionless* drag for drift and shift distributions is the same, the *collisional* drag force for the drift distribution exceeds that for the shift distribution by roughly a factor of 2.

The collisional drag force enhancement can be represented by an almost universal function of scaled collisionality and flow velocity, for which simple fits are provided.

ACKNOWLEDGMENTS

Work supported in part by NSF/DOE Grant DE-FG02-06ER54982. C B Haakonsen was supported in part by the Department of Energy Office of Science Graduate Fellowship Program (DOE SCGF), administered by ORISE-ORAU under contract no. DE-AC05-06OR23100. Some of the computer simulations were carried out on the MIT PSFC parallel AMD Opteron/Infiniband cluster Loki, concerning which we thank John Wright and Darin Ernst for advice.

REFERENCES

- ¹S. Chandrasekhar, Ap. J. **97**, 255 (1943)
- ²R. Cohen, L. Spitzer, and P. Routly, Physical Review **80**, 230 (Oct. 1950), ISSN 0031-899X, <http://link.aps.org/doi/10.1103/PhysRev.80.230>
- ³M. Rosenbluth, W. MacDonald, and D. Judd, Physical Review **107**, 1 (Jul. 1957), ISSN 0031-899X, <http://link.aps.org/doi/10.1103/PhysRev.107.1>
- ⁴M. D. Kilgore, J. E. Daugherty, R. K. Porteous, and D. B. Graves, Journal of Applied

- Physics **73**, 7195 (1993), ISSN 00218979, <http://link.aip.org/link/JAPIAU/v73/i11/p7195/s1&Agg=doi>
- ⁵R. L. Liboff, *Physics of Fluids* **2**, 40 (Jan. 1959), ISSN 00319171, <http://link.aip.org/link/?PFLDAS/2/40/1>
- ⁶T. Kihara, *J. Phys. Soc. Japan* **14**, 402 (1959)
- ⁷E. A. Mason, R. J. Munn, and F. J. Smith, *Phys. Fluids* **10**, 1827 (1967)
- ⁸H.-S. Hahn, E. A. Mason, and F. J. Smith, *Phys. Fluids* **14**, 278 (1971)
- ⁹S. Khrapak, A. Ivlev, G. Morfill, and H. Thomas, *Physical Review E* **66**, 2 (Oct. 2002), ISSN 1063-651X, <http://link.aps.org/doi/10.1103/PhysRevE.66.046414>
- ¹⁰J. E. Daugherty, R. K. Porteous, M. D. Kilgore, and D. B. Graves, *Journal of Applied Physics* **72**, 3934 (1992), http://ieeexplore.ieee.org/xpls/abs_all.jsp?arnumber=5144269
- ¹¹S. J. Choi and M. J. Kushner, *Plasma Science, IEEE Transactions on* **22**, 138 (1994), http://ieeexplore.ieee.org/xpls/abs_all.jsp?arnumber=279017
- ¹²I. H. Hutchinson, *Plasma Physics and Controlled Fusion* **47**, 71 (Jan. 2005), ISSN 0741-3335, <http://stacks.iop.org/0741-3335/47/i=1/a=005?key=crossref.6ff08f498dcf905c7a5f23113af0dcae>
- ¹³I. H. Hutchinson, *Plasma Physics and Controlled Fusion* **48**, 185 (Feb. 2006), ISSN 0741-3335, <http://stacks.iop.org/0741-3335/48/i=2/a=002?key=crossref.52c77ab504cab195fe503e7fc4053592>
- ¹⁴S. Khrapak, a. Ivlev, G. Morfill, and S. Zhdanov, *Physical Review Letters* **90**, 1 (Jun. 2003), ISSN 0031-9007, <http://link.aps.org/doi/10.1103/PhysRevLett.90.225002>
- ¹⁵S. A. Khrapak, A. V. Ivlev, S. K. Zhdanov, and G. E. Morfill, *Phys. Plasmas*, 42308(2005)
- ¹⁶H. Fahr and K. G. Mueller, *Zeitschrift fuer Physik* **200**, 343 (Aug. 1967), ISSN 1434-6001, <http://link.springer.com/10.1007/BF01326177>
- ¹⁷F. Rebertrost, *Chemical Physics Letters* **17**, 15 (1972), <http://www.sciencedirect.com/science/article/pii/0009261472850863>
- ¹⁸A. V. Ivlev, S. K. Zhdanov, S. A. Khrapak, and G. E. Morfill, *Physical Review E* **71**, 016405 (2005), <http://pre.aps.org/abstract/PRE/v71/i1/e016405>
- ¹⁹L. Patacchini and I. H. Hutchinson, *Physical Review Letters* **101**, 1 (Jul. 2008), ISSN 0031-9007, <http://link.aps.org/doi/10.1103/PhysRevLett.101.025001>
- ²⁰M. Lampe, T. B. Rocker, G. Joyce, S. K. Zhdanov, A. V. Ivlev, and G. E. Morfill, *Physics of*

- Plasmas **19**, 113703 (2012), ISSN 1070664X, <http://link.aip.org/link/PHPAEN/v19/i11/p113703/s1&Agg=doi>
- ²¹J. Neufeld and R. Ritchie, Physical Review **98**, 1632 (1955), http://prola.aps.org/abstract/PR/v98/i6/p1632_1
- ²²A. Ivlev, S. Khrapak, S. Zhdanov, G. Morfill, and G. Joyce, Physical Review Letters **92**, 1 (May 2004), ISSN 0031-9007, <http://link.aps.org/doi/10.1103/PhysRevLett.92.205007>
- ²³M. Lampe, G. Joyce, G. Ganguli, and V. Gavrishchaka, Phys. Plasmas **7**, 3851 (2000), ISSN 1070664X, <http://link.aip.org/link/PHPAEN/v7/i10/p3851/s1&Agg=doi>
- ²⁴M. Lampe, G. Joyce, and G. Ganguli, IEEE Trans. Plasma Sci. **33**, 57 (2005)
- ²⁵I. H. Hutchinson, Phys. Plasmas **18**, 32111 (2011)
- ²⁶R. L. Dewar and D. Leykam, Plasma Physics and Controlled Fusion **54**, 014002 (Jan. 2012), ISSN 0741-3335, <http://stacks.iop.org/0741-3335/54/i=1/a=014002?key=crossref.d775fa4ceed15dea2ccafe7ca3b146f6>
- ²⁷P. Ludwig, W. J. Miloch, H. Kählert, and M. Bonitz, New Journal of Physics **14**, 053016 (May 2012), ISSN 1367-2630, <http://stacks.iop.org/1367-2630/14/i=5/a=053016>
- ²⁸I. H. Hutchinson, Physical Review Letters **107**, 2 (Aug. 2011), ISSN 0031-9007, <http://link.aps.org/doi/10.1103/PhysRevLett.107.095001>
- ²⁹I. H. Hutchinson, Physical Review E **85**, 1 (Jun. 2012), ISSN 1539-3755, <http://link.aps.org/doi/10.1103/PhysRevE.85.066409>
- ³⁰I. H. Hutchinson, Plasma Physics and Controlled Fusion **44**, 1953 (Sep. 2002), ISSN 0741-3335, <http://stacks.iop.org/0741-3335/44/i=9/a=313?key=crossref.0642ea953e906cb5fc09bd8cafcd76>
- ³¹I. H. Hutchinson, Plasma Physics and Controlled Fusion **45**, 1477 (Aug. 2003), ISSN 0741-3335, <http://stacks.iop.org/0741-3335/45/i=8/a=307?key=crossref.3f02ffa206df98c02b0a1de95b8686e5>
- ³²C. K. Birdsall and A. B. Langdon, *Plasma Physics via Computer Simulation* (IOP Publishing, Bristol, 1991)
- ³³I. H. Hutchinson, Arxiv, 1105:1356(May 2011), arXiv:1105.1356, <http://arxiv.org/abs/1105.1356>
- ³⁴S. A. Khrapak, A. V. Ivlev, G. E. Morfill, S. K. Zhdanov, and H. M. Thomas, IEEE Trans. Plasma Sci. **32**, 555 (Apr. 2004), ISSN 0093-3813, <http://ieeexplore.ieee.org/>

lpdocs/epic03/wrapper.htm?arnumber=1308514

³⁵For very high values of β , the collection radius can be no larger than a few λ or else the OML validity conditions are violated³⁴. This limitation proves to be unimportant for the high flow velocities at which the direct collection is an important fraction of the force.

³⁶Y. L. Al’pert, A. V. Gurevich, and L. P. Pitaevskii, *Space Physics with Artificial Satellites* (Consultants Bureau, New York, 1965)

³⁷Actually in¹³ the denominator of the cubic term consisted of three terms to accommodate floating potential variation due to ion mass changes, and ion temperature variation: $[0.6 + 0.05 \ln(m/Z) + (\lambda_{De}/5r_p)(\sqrt{T_i/ZT_e} - 0.1)]c_s$. The simplification to the present expression improves the fit, especially in the vicinity of $v_f \sim 0.2c_s$. We are not here investigating changes in grain potential.

³⁸L. Patacchini and I. H. Hutchinson, *Phys. Plasma* **16**, 62101 (2009)

³⁹See supplementary material at [URL to be inserted by AIP] which provides computer routines for force evaluation.